A reactivity-based probe of the intracellular labile ferrous iron pool

Benjamin Spangler[1], **Charles W. Morgan**[1], **Shaun D. Fontaine**[1], **Mark N. Vander Wal**[2], **Christopher J. Chang**[2,3], **James A. Wells**[4,5], and **Adam R. Renslo**[4]

[1]Graduate Program in Chemistry & Chemical Biology, University of California, San Francisco, California

[2]Departments of Chemistry and Molecular and Cell Biology, University of California, Berkeley

[3]Howard Hughes Medical Institute, University of California, Berkeley

[4]Department of Pharmaceutical Chemistry, University of California, San Francisco, California, USA

[5]Department of Cellular and Molecular Pharmacology, University of California, San Francisco, California, USA

Abstract

Improved methods for studying intracellular reactive iron(II) are of significant interest for studies of iron metabolism and disease relevant changes in iron homeostasis. Here we describe a highly-selective reactivity-based probe in which Fenton-type reaction with intracellular labile iron(II) leads to unmasking of the aminonucleoside puromycin. Puromycin leaves a permanent and dose-dependent mark on treated cells that can be detected with high sensitivity and precision using the high-content, plate-based immunofluorescence assay described. Using this new probe and screening approach, we detected alteration of cellular labile iron(II) in response extracellular iron conditioning, overexpression of iron storage and/or export proteins, and post-translational regulation of iron export. Finally, we utilized this new tool to demonstrate the presence of augmented labile iron(II) pools in cancer cells as compared to non-tumorigenic cells.

Keywords

Reactivity-Based Probe; Labile Iron Pools; Iron Metabolism

Introduction

Iron co-factors are required for various essential enzymatic functions, including *de novo* nucleotide synthesis, cell cycle regulation, maintenance of genomic stability, and mitochondrial respiration[1,2,3]. Redox cycling between ferric (Fe^{III}) and ferrous (Fe^{II}) iron is exploited by these enzymes to complete their catalytic cycles[3]. However, redox active iron can also promote the disproportionation of hydrogen peroxide (Fenton reaction) to produce hydroxyl and hydroperoxyl radicals - reactive oxygen species (ROS) that confer cellular damage and can lead to apoptosis[4–7]. Accordingly, iron homeostasis is rigorously regulated to ensure that cells can produce the iron co-factors required to support essential enzyme function, while limiting exposure to ferritoxic species[8–10].

Iron homeostasis at the level of the cell is maintained through a balance of iron import, storage, and export. Linking these nodes of iron metabolism is a pool of mostly cytosolic, redox active iron referred to as the labile (or "chelatable") iron pool. Changes to this labile iron pool are relevant in many disease states including prion diseases[11], inflammation[12], and cancer[1]. Rapidly proliferating cells are expected to possess augmented labile iron pools as a result of their increased requirements for DNA synthesis, repair, and mitochondrial respiration. Indeed, iron acquisition and export pathways are altered in many cancer cells in ways that predict for increased labile iron[13–16]. Excess iron has been shown to contribute to tumor initiation and growth[13,17], and epidemiological evidence has established links between changes in iron metabolism and clinical outcomes in cancer patients[15,18]. The ability to study the labile, reactive iron pool and understand how various factors influence it is thus of significant interest.

Previous attempts to quantify labile iron concentrations have focused on fluorescent probes like Calcein AM and PhenGreen SK that possess metal-binding moieties. While such reagents are not intrinsically selective for binding of iron, their fluorescence is partially quenched upon binding iron. Subsequent sequestration of the bound iron with a (non-fluorescent) iron chelator such as 2,2′-bipyridyl is then used to infer labile iron concentrations based on the extent of de-quenching, and reference to some *in situ* or *ex situ* fluorescence calibration standard. The significant challenges and caveats associated with these existing tools and approaches have been comprehensively reviewed[19–21]. More recently, fluorescent "turn-on" probes for ferrous iron have been reported. RhoNox-1[22] and IP-1[23,24] are designed to be activated upon the iron(II)-promoted reduction of an N–O or C–O bond in a fluorescein-type dye. These probes thus represent "reactivity-based" probes in which a reaction promoted by the analyte (ferrous iron) produces a detectable response.

We hypothesized that a new class of reactivity-based probes for Fe(II) might be developed around the Fenton reaction, which involves the iron(II)-dependent reduction of a peroxide bond. A peroxidic probe of this type would need to react selectively with Fe(II) and produce an easily detectable signal. While we judged simple organic peroxides too reactive for such purposes, the 1,2,4-trioxolane ring embedded in the antimalarial agents arterolane[25,26,27] and artefenomel[28] combines good chemical stability with finely-tuned Fe(II)-dependent reactivity[29–32]. Accordingly, we re-engineered the arterolane scaffold so that Fenton reaction of the endoperoxide bond is mechanistically coupled to traceless release of amine-tethered

payloads[33–35]. For detection of labile iron pools, we imagined employing this scaffold for the Fe(II)-dependent unmasking of either fluorescent moieties or cell-active compounds such as puromycin, an aminonucleoside that leaves a permanent mark on the cell that can be detected with α-puromycin antibodies.

Here we describe a novel reactivity-based probe of labile iron(II) pools and a companion high-throughput immunofluorescence assay that allows even subtle changes in labile iron concentrations to be discerned. We further demonstrate the selectivity of this probe for reaction with intracellular Fe(II) over other metals or changes to intracellular redox status. Using this approach, we detected alteration of labile iron pools in response to extracellular iron conditioning, overexpression of iron storage and/or export proteins, and post-translational down-regulation of iron export by the peptide hormone hepcidin. Finally, we demonstrated the presence of augmented labile iron pools in cancer cells as compared to non-tumorigenic cells in cell culture experiments. Overall, this work presents a sensitive and selective new method for studying labile iron(II) pools and suggests a new approach for tumor-selective drug delivery.

Results

Developing trioxolane-based probes of ferrous iron

Developing a reactivity-based probe of the ferrous iron pool required mechanistically linking reduction of the Fe(II)-reactive 1,2,4-trioxolane moiety to a readily observable and quantifiable output. We reasoned that this might be achieved with a probe in which Fe(II)-induced trioxolane fragmentation served to dissociate a FRET pair (Fig. 1a). Thus, we synthesized probe **1** in which a fluorophore-quencher pair is separated by a trioxolane scaffold derived from arterolane (Fig. 1a). As expected, we found the DANSYL moiety in probe **1** to be internally quenched, with negligible fluorescence signal observed when excited at the absorbance maximum (337 nm) (Fig. 1b). Upon exposure to Fe(II) species however, a strong fluorescence signal with an emission maximum at 465 nm appeared in a time and concentration dependent fashion (Fig. 1b). Significantly, compound **1** exhibited negligible reactivity with Fe(III) or other biologically relevant metal ions, even at very high (1.5 mM) concentrations (Fig. 1c, Supplementary Results, Supplementary Fig. 1). Similarly, treatment with transferrin-bound Fe(III), or biologically relevant oxidants or reductants did not produce significant activation of **1** (Fig. 1d, Supplementary Fig. 1). While these studies were invaluable for demonstrating the Fe(II)-specific reactivity of the 1,2,4-trioxolane moiety, compound **1** was not useful for studies in intact cells due to poor cellular permeability.

A cell-active probe (**3**) was ultimately produced by conjugating puromycin (**2**) to our previously described[33,34] 1,2,4-trioxolane scaffold (Fig. 2a, Supplementary Note). Puromycin is incorporated in nascent polypeptides at the ribosome, producing a permanent and dose-dependent mark on cells that can be detected with anti-puromycin antibodies. Significantly, the α-amino group of puromycin (**2**) required for incorporation in peptides is carbamoylated in conjugate **3** and thus puromycin incorporation from **3** is precluded prior to reaction with Fe(II). As an important negative control we prepared the bioisosteric but non-

peroxidic dioxolane conjugate **4**[35], which is unreactive with Fe(II) (Fig. 2a, Supplementary Note).

Incubation of **3** in cell culture media for 24 hours at 37 °C produced no observable release of **2**, demonstrating good stability under cell culture conditions in the absence of Fe(II) (Supplementary Fig. 2a). When ferrous ammonium sulfate (FAS) was added to the media however, the trioxolane ring in **3** fragmented completely within 30 minutes to yield the expected ketone intermediate **5** (Fig. 2b). Intermediate **5** then underwent spontaneous retro-Michael reaction to produce **2**, confirming that when exposed to reactive Fe(II)-species in solution, probe **3** releases free puromycin (**2**) as intended (Fig. 2b).

Detection of intracellular ferrous iron with probe 3

To determine if probe **3** could report on labile Fe(II) pools in mammalian cells, we compared the rate and extent of puromycin (**2**) incorporation over 24 hours in U-2 OS cells treated with equimolar concentrations of **2** or probe **3**. Encouragingly, we observed a time-dependent increase in puromycin incorporation in cells treated with **2** or **3**, as determined by Western and dot blot analysis with α-puromycin antibodies (Fig. 2c–d). Cells treated with **3** showed a slight lag in puromycin incorporation compared to those treated with free puromycin (**2**), likely reflecting the rate-limiting release of **2** from retro-Michael intermediate **5** in **3**-treated cells. Total levels of incorporation at 24 hours were nearly identical however, consistent with the efficient intracellular release of **2** from **3** mediated by intracellular labile Fe(II). By contrast, puromycin incorporation was undetectable in U-2 OS cells treated with dioxolane-puromycin control **4**, indicating that intracellular release of puromycin from **3** is peroxide dependent (Fig. 2c–d).

To characterize the response of **3** under a broader range of conditions, we developed a robust, cell based immunofluorescence assay using high-content imaging with single cell resolution. This high-throughput assay allowed us to study the time and dose dependence of the cellular effects of **3** by visualizing cellular puromycin incorporation in single cells and then quantifying exposure across hundreds to thousands of cells using high content image analysis (Fig. 2e–g). We found that U-2 OS cells treated with equimolar concentrations (0.1 μM) of probe **3** or free puromycin (**2**) showed similar incorporation half-lives (2.5 h and 2.0 h respectively) and fluorescence saturation points (441 vs 496 AU), indicating that activation of **3** and release of **2** occurs rapidly and efficiently within cells (Fig. 2f). Interestingly, the rate-limiting retro-Michael reaction of intermediate **5** to liberate **2** appears to be appreciably accelerated in cells (Fig. 2c–f) when compared to cell-free media containing Fe(II) (Fig. 2b). While the reason(s) for this are unclear, we have observed similarly accelerated rates of intracellular retro-Michael reaction of trioxolane conjugates in malaria parasites[33,35], suggesting a common feature of both environments may enhance the rate of the β-elimination. Consistent with the analysis by Western blotting, U-2 OS cells treated with non-peroxidic control **4** showed negligible immunofluorescence signal in the high-content assay, further confirming that puromycin release from **3** is peroxide dependent (Fig. 2f–g). As the permeability rates of **2** and **3** were found to be very similar in a parallel artificial membrane permeability assay (PAMPA), we expect that rates of puromycin incorporation for **2** and **3** are not significantly affected by differential cellular uptake (Supplementary Table 1).

Sensitivity and iron selectivity of probe 3

To determine whether **3** could be used to detect changes in intracellular Fe(II) concentrations, PC-3 cells were pre-treated for two hours with various concentrations of ferrous ammonium sulfate (FAS) or the iron chelator 2,2′-bipyridyl (Bpy) in serum free media, washed, and then probed with 1 μM **3** for four hours. The cells pre-treated with FAS showed dose dependent increases in signal from puromycin incorporation compared to cells that were pre-treated with vehicle (Fig. 3a–b and Supplementary Fig. 3). Pre-conditioning with even low μM concentrations of FAS produced a statistically significant response over control, demonstrating that probe **3** exhibits excellent sensitivity to changes in intracellular Fe(II) levels. Cells treated with Bpy correspondingly showed a dose-dependent decrease in signal from puromycin incorporation, as expected, and consistent with Fe(II)-dependent activation of **3** (Fig. 3a–b and Supplementary Fig. 3). An analogous dose-dependent decrease in immunofluorescence was also observed when PC-3 cells were treated with the iron chelator DFO[19,20,22,36] rather than Bpy (Supplemental Fig. 4a). When PC-3 cells pre-conditioned with FAS or DFO were treated with free **2** instead of **3**, no changes in the immunofluorescence signal were observed, indicating that these pre-treatments do not affect rates of protein synthesis or puromycin incorporation but rather the rate and extent of puromycin release from **3** (Supplementary Fig. 4a). Neither did these treatments affect cell viability under the conditions employed (Supplementary Fig. 4b). Further analysis of pre-conditioned and vehicle-treated cells revealed a significant distribution in the response of individual cells within the population. Thus, FAS pre-treatment further increased the distribution of responses (compared to controls) while Bpy treatment dramatically reduced the distribution, which converged on the minimal signal in the assay (Supplementary Fig. 4c). In neither pre-conditioned cells nor controls was the overall response to **3** driven by a small population of highly responsive cells.

To provide further evidence that probe **3** is responding to changes in intracellular Fe(II) and not other metal ions, we performed an analogous set of pre-conditioning experiments, applying various biologically relevant metal ions (Fig. 3c). Thus, PC-3 cells were pre-treated in dose response with various metal ions in serum-free media for two hours, washed, and probed with **3** (1 μM) for four hours, and then fixed, stained, and imaged. From these experiments, only cells pre-treated with Fe(II) or Fe(III) elicited a notable response from probe **3** at any of the tested concentrations (Fig. 3c and Supplementary Fig. 5). Since **3** is unreactive with Fe(III) (Supplementary Fig. 2b)[30], the robust response in cells pre-treated with Fe(III) reflects an increase in intracellular Fe(II) following internalization and reduction of the applied Fe(III), as would be expected based on current understanding of cellular iron acquisition mechanisms[1,37].

To confirm that probe **3** is selective for Fe(II) over other biologically relevant reductants, PC-3 cells were treated with various reagents previously shown to alter intracellular glutathione (GSH) levels and redox status. The concentrations and manner of application were based on those reported previously for the various reagents[38–43]. Notably, none of these conditions produced any substantial, dose-dependent effects on signal from puromycin release in cells treated with **3** (Fig. 3d, Supplementary Fig. 5a–b), a result that is consistent with the observed stability of FRET probe **1** to the same reagents *in vitro* (Fig. 1d). To verify

that pre-treatment with GSH, *N*-acetyl cysteine (NAC), or the glutathione synthesis inhibitor buthionine sulfoximine (BSO) in fact altered intracellular GSH concentrations, we employed a commercial fluorometric GSH detection kit. While the various pre-treatments substantially altered intracellular GSH concentrations as expected, the effects on signal from **3** were minor (ca. 10% or less change from control) and did not track with the observed dose dependent changes to GSH levels (Supplementary Fig. 5c–d). These results, together with the metal ion selectivity data presented above, indicate that probe **3** is a highly sensitive and selective probe of intracellular labile ferrous iron.

Comparing 3 with turn-on probes IP1 and RhoNox-1

Next we compared the sensitivity of probe **3** and immunofluorescence detection with the recently reported fluorescent turn-on probes IP-1 and RhoNox-1. We compared the response of IP-1 and RhoNox-1 in pre-conditioned PC-3 cells using the same high-throughput high-content imaging approach described above for studies of **3**. Conditions for iron pre-conditioning were identical to those used with **3** and probe application for IP-1 (2 μM, 2 h) and RhoNox-1 (5 μM, 4h) were adapted from the conditions reported previously, with some optimization. All three probes produced a qualitatively similar response following pre-treatment with high concentrations (0.3 mM) of Bpy or FAS, however, the magnitude of response under all conditions was notably higher with **3** (Fig. 3e). Upon pre-treating cells with lower concentrations of Bpy or FAS, probe **3** was still able to detect subtle but statistically significant changes to labile iron(II) pools (Supplementary Fig. 6). Finally, only probe **3** was able to detect changes to iron pools induced by the peptide hormone hepcidin (HP), a post-translational regulator of the iron exporter ferroportin (Fig. 3e). Thus, probe **3** detected increased labile iron(II) in cells treated with 1 μg/mL of HP in cell culture media for 16 h prior to and during FAS pre-treatment, the expected result for cells with reduced export capacity induced by HP treatment (Fig. 3e). This effect of HP treatment was detected at all doses of FAS studied with probe **3** (Supplementary Fig. 6). These findings are consistent with previous observations using IP-1 to monitor changes to the labile iron pool induced by HP and FAS using lower throughput confocal microscopy methods[23]. Immunofluorescence imaging with probe **3** thus affords greater sensitivity than fluorescence imaging with IP-1 and RohNox1 in the context of a high-throughput plate-based based imaging assay. The advantages of the latter approach include the ability to image large fields of cells (2,000–10,000 cells per condition) with single-cell resolution and to simultaneously explore multiple treatment conditions in parallel by employing cells seeded in 96- or 384-well plates.

Profiling the reactive iron pool across cell lines

Having established the utility of trioxolane-puromycin conjugate **3** as a selective and sensitive probe of intracellular labile iron(II), we sought to test the hypothesis that labile iron pools are augmented in cancers. We thus compared the labile iron(II) pools of selected cancer cell lines with non-tumorigenic cells using **3**. We found that the immunofluorescence response of **3** in non-tumorigenic MCF10A cells was significantly diminished as compared to that of **3** in RKO cells (Fig. 4a–b). Because different cell lines may differ in rates of protein synthesis and puromycin incorporation, we normalized the maximal fluorescence

signal in cells treated with probe **3** to that in cells treated with equimolar puromycin (**2**). This provided a convenient metric – normalized signal (%) - to compare Fe(II) pools across cell lines. We profiled additional cancer cell lines and a second non-tumorigenic cell line (IMR-90) using this methodology and found the cancer cell lines exhibited normalized signal values of ~75–90% as compared to ~40–45% for the non-tumorigenic cell lines (Fig. 4c and Supplemental Fig. 7). Thus, across a small panel of cell lines, probe **3** detected augmented pools of labile Fe(II) in cancer cell lines as compared to non-tumorigenic cell lines, consistent with current notions of iron homeostasis in cancer.

Genetic modulation of the reactive iron pool

To evaluate the potential utility of probe **3** for studying regulatory mechanisms of iron homeostasis, we explored whether ectopic expression of ferritin heavy chain (FTH-1) and/or ferroportin (SLC40A1) would produce the expected reduction in labile iron(II) concentrations. We selected RKO cells for these studies because these cells have low endogenous levels of both proteins and a substantial labile iron(II) pool as determined with **3** (Fig. 4c, Supplementary Fig. 8). We found that ectopic expression of either FTH-1 or SLC40A1 by transient transfection of RKO cells resulted in modest but significant decreases in the reactive iron pool as determined with **3** (Fig. 4d). Co-transfection with both FTH-1 and SLC40A1 decreased labile iron concentrations more dramatically, consistent with the orthogonal roles of these two proteins in iron sequestration and export (Fig. 4d). Thus, the combination of probe **3** and high-throughput immunofluorescence imaging represents a useful new methodology for assessing labile iron(II) pools in studies of cellular homeostasis and iron metabolism.

Discussion

Studies of iron metabolism and intracellular labile iron pool have traditionally relied on fluorescent probes like Calcein-AM and PhenGreen-SK with iron chelators like deferoxamine and deferiprone[19,20,44]. However, Calcein and PhenGreen lack intrinsic binding selectivity for iron over other metals (e.g. Ca^{2+}, Zn^{2+}, Mg^{2+}) and are experimentally challenging to use[21]. At the same time, iron chelators like DFO and deferiprone bind Fe(III) much more avidly than Fe(II) and can even compete for Fe(III) bound to ferritin, artificially perturbing the homeostatic system being studied[21]. Herein we have described a new reactivity-based probe (**3**) that directly interrogates labile intracellular Fe(II) via the iron(II)-dependent reaction of a hindered trioxolane species. In contrast to traditional tools like DFO, probe **3** is useful at non-cytotoxic nanomolar concentrations and its novel mechanism of action involves neither the binding nor sequestration of the Fe(II) species being interrogated.

We also describe a high-content, plate-based immunofluorescence assay for puromycinylated proteins that has been optimized for applications involving probe **3**. Using this new methodology it will be possible to study large numbers of chemical and/or genetic manipulations and their corresponding effects on the labile iron(II) pool in parallel using automated processes. The results described herein demonstrate that **3** can be used to detect even subtle changes in labile iron pools with significantly greater sensitivity than is

achievable with previously reported reactivity-based fluorescent probes of Fe(II) under comparable conditions[22,23].

Using the described methodology we observed increased sensitivity to exogenous iron treatment induced by post-translational modulation of ferroportin levels with the biologically relevant peptide hormone hepcidin. Similarly, probe **3** detected diminished labile iron(II) pools in cells ectopically expressing iron export and storage proteins. The impact of these genetic manipulations (separately or in combination) on labile iron(II) could be assessed quantitatively using **3**. Comparison of labile iron(II) pools across diverse cell lines revealed that the cancer cells profiled had significantly augmented iron pools compared to non-tumorigenic cells, a finding that is consistent with current thinking around iron metabolism and its dysregulation in cancer[1].

Additional advantages of **3** and antibody-based puromycin detection include the flexibility to change the nature of the primary or secondary antibody employed for detection. Thus, in place of the fluorescent secondary antibodies employed herein, the assay could be readily adapted to use primary or secondary antibodies conjugated to various radiolabels, enzymes, or nanoparticles, etc. This flexibility should permit probe **3** to be deployed in diverse scenarios with application-specific optimization of the puromycin detection methodology. Also, since puromycin incorporation is irreversible and occurs secondary to reaction with Fe(II), the analysis of fixed cells can be performed at leisure without concern of time-dependent loss of Fe(II)-specific signal. Given the excellent sensitivity and high-throughput nature of the assays described, probe **3** should find general utility in studies of iron metabolism and cellular homeostasis.

Finally, our findings with **3** suggest the potential of iron(II)-dependent drug delivery as a therapeutic strategy in cancer. Given that we observed augmented labile iron pools in multiple cancer cell lines from diverse origins, such a therapeutic strategy could have broad implications for cancer chemotherapy. Our current efforts are thus focused on studying and leveraging differences in labile iron concentrations between normal cells/tissues and the tumor environment for selective delivery of chemotherapeutic agents.

Online Methods

General Procedures and Materials

Fluorescence and absorbance data was collected on a Molecular Devices Flex Station 3. Automated cell imaging was conducted using a GE IN Cell2000 automated cell imager. Mammalian cell lines were obtained from ATCC unless otherwise indicated and maintained in an atmosphere of 5% CO_2 in Dulbecco's Modified Eagle Medium (DMEM) or RPMI 1640 media purchased from HyClone supplemented with 10% FBS (Gibco), Pen/Strep (1x final concentration, Gemini Bio-Products), and non-essential amino acids (UCSF Cell Culture Facility) as recommended. MCF10a derived cell lines were graciously provided by the Bandyopadhyay lab at UCSF and cultured as previously reported[45]. Cell lines were checked annually for mycoplasma contamination.

All Western Blot and Dot Blot images were analyzed with Licor Image Studio Software to determine signal intensity. Graphing and analysis of data was done using GraphPad Prism 6 Software and Microsoft Excel 2010. Figures were prepared with Adobe Design Standard CS6 software.

Reagents—Puromycin Dihydrochloride (>99%) was purchased from P212121. Zinc Sulfate was purchased as a 100 mM aq. Soln. from Alfa Aesar. Cobalt(II) sulfate heptahydrate (>99%) was purchased from Sigma-Aldrich: SIAL. Magnesium(II) chloride hexahydrate (ACS grade, >99%) was purchased from Amresco. Ferrous ammonium sulfate (99%) was purchased from Santa Cruz Biotechnology. Sodium chloride (99.5%) was purchased from Fisher Scientific. Nickel(II) sulfate (99.99%), Fe(II) bromide (98%), Fe(III) sulfate hydrate (97%), copper(II) chloride (99.999%), copper(I) chloride (>99.995%), calcium chloride (>97%), potassium chloride (>99%), and manganese(II) chloride (98%) were all purchased from Sigma Aldrich. N-acetyl cysteine (NAC) was purchased from TCI America (>98%). Ascorbic Acid was purchased from Chem Impex Int'l (99.8%). Buthionine sulphoximine (BSO) (>98%) was purchased from Cayman Chemical and β-mercaptoethanol (BME) (>98%) was purchased from BioRad. Hepcidin was purchased from abcam (1 mg/mL, 70–90%).

Statistics—Error bars in all figures represent s.e.m. unless otherwise indicated. When three or more means were compared, one or two-way ANOVA tests were applied as required with Dunnett's multiple comparisons tests used to determine significance. Statistical significance is indicated as follows: * = P 0.05, ** = P 0.01, *** = P 0.001, **** = P 0.0001.

Fluorescence Assays of 1—Solutions of the indicated metal ions as sulfate, chloride, or bromide salts were prepared in milli-Q purified water to the specified concentrations (2x stock). 10 μL of each of these solutions was added to 10 μL of a 30 μM solution of **1** in DMSO in white, low volume, flat bottom 384-well plates (Corning, #3824) and mixed thoroughly. The fluorescence signal at E_{max} (465 nm) for each well when excited at 337 nm was then measured every five minutes for 2–5 hours. Rates of fluorescence increase were determined for each sample using the initial rate method and compared to determine reactivity.

In vitro Fragmentation Studies—Solutions of trioxolane conjugates in DMSO (10 mM) were spiked into 1 mL of RPMI cell culture media (supplemented as in cell culture studies) which had been warmed with stirring to 37 °C to give a final solution of 300 μM compound with 3% DMSO co-solvent which was stirred at 37 °C. Aliquots were taken at various time points and analyzed by LC/MS. The chromatography method involved gradient elution from 0–95% MeOH in water (constant 0.1% formic acid) over 8 min. Stability of the compounds was followed by observing signal at absorbance maxima (**2**: λ = 275) of the peaks corresponding to the parent compounds and free payloads as determined by authentic samples. For iron conditioned samples 0.5 mL of 0.6 mM solutions of compound in DMSO were spiked into 0.5 mL of RPMI cell culture media containing 60 mM FAS while stirring at

37 °C. 50 µL aliquots of the resulting mixture were removed periodically and analyzed via LC/MS for trioxolane fragmentation and release of free payload.

Western Blots—Cells were plated at 300,000 cells per well in 6-well plates and grown to confluence. Media was then removed, cells were washed twice with PBS, and 200 µL of RIPA lysis buffer containing sigma protease inhibitor cocktail (P8340, 1:100) was added to each well. Cells were incubated in lysis buffer for 10 min at RT then scrapped and collected. Lysates were analyzed by BCA and normalized for total protein content with lysis buffer then denatured in Laemmli loading buffer with 0.01 M DTT at 100 °C for 10 min. 10 µg of protein from each sample was then loaded onto Biorad Mini-PROTEAN® TGX™ 4–15% gels and run @ 150V for 55 min then transferred to Immobilon PVDF membrane at 35 V for 1 h. The membrane was blocked with 5% non-fat milk in TBS-T for 1 h at rt then incubated with the indicated antibodies in 2.5% non-fat milk overnight at 4 °C. The blot was then washed three-times with TBS-T and once with PBS-T before incubating with Licor IRDye secondary antibodies in Odyssey blocking buffer (#927-40000) + 0.2% Tween-20 and 0.01% Sodium dodecyl sulfate (SDS). The blot was washed 3 times with PBS-T for 5 min and once with PBS then imaged for fluorescent signal on an Odessey Classic Infrared Imaging System. Ferritin antibodies were obtained from Abcam (Ab75973) and tubulin antibodies were obtained from Sigma (T6199).

Dot Blots—Samples prepared as for Western Blots were spotted on to Immobilon PVDF membrane which was activated with MeOH then allowed to dry completely prior to spotting 1 µg of total protein per sample. Samples were allowed to completely adsorb onto the membrane and dry before blocking with with 5% non-fat milk in TBST for 1 h at rt and then staining and imaging as done in Western Blots.

Puromycin incorporation via in cell immunofluorescence—Cells were plated in 96-well greiner black µClear tissue culture plates at 4,000–7,000 cells per well and incubated at 37 °C in 5% CO_2 incubators for 24 h (or until ca. 80% confluent) prior to exposure to compounds. Cells were then exposed to puromycin (**2**) or conjugates thereof (**3**,**4**) at the specified concentrations (diluted in cell culture media from 1000x DMSO stocks) in media for the indicated periods of time prior to removing media, washing cells with PBS, and fixing cells in 4% paraformaldehyde for 10 min at rt then washing twice with PBS and once with PBS containing 0.1% Triton X-100. Cells were then stained with Kerafast α-puromycin antibody [3RH11] (1:500) in 10% FBS in PBS with 0.1% Triton X-100 for 30 min at 37 °C. Cells were washed once with PBS and once with PBS containing 0.1% Triton X-100 then stained with α-mouse secondary FITC (488 nm excitation, 535 nm emission) antibody (1:100) and Hoechst nuclear stain at a final concentration of 10 µg/mL in 10% FBS in PBS with 0.1% Triton X-100 for 30 min at 37 °C. Cells were washed once with PBS containing 0.1% Triton X-100 and once with PBS then stored in PBS and imaged using an IN Cell 2000 automated cell imager at 10x magnification with 6–9 images per well in FITC and DAPI channel fluorescence. Images were analyzed for nuclei count and puromycin incorporation by IN Cell developer software. Puromycin incorporation was assessed by mean cellular fluorescence density in the FITC channel for each cell as defined by targets seeded with nuclei in the DAPI channel (ca. 2,000–9,000 cells per condition).

Average cellular fluorescence density under each condition was determined and reported values represent the well mean average across triplicates +/− s.e.m. unless otherwise indicated. Background signal from cells treated with DMSO instead of **2** or **3** was subtracted for each condition. For cross cell line comparisons and genetic modulation experiments signal in cells treated with the trioxolane-conjugate **3** was normalized to that in cells treated with free puromycin (**2**) and reported as percent of labelling at saturation unless otherwise indicated.

Iron Conditioning—Stock solutions of ferrous ammonium sulfate (FAS) were prepared in deionized water immediately before dosing then diluted into cell culture medium to the desired final concentrations. Cells were exposed to the indicated doses of FAS, or the iron chelators DFO or Bpy (from DMSO stocks), in RPMI 1640 cell culture medium in 96-well plates for 2 h and then washed with PBS to remove any residual extracellular iron. Cells were then treated with a 1 μM solution of **2** or **3** in cell culture medium for 4 h. Cells treated with iron chelators (DFO and Bpy) were continually exposed to the chelator to prevent the cell from mobilizing iron stores and replenishing the labile Fe(II) pool during the course of treatment with **3.** Post-treatment cells were washed, fixed, and stained as in the puromycin incorporation studies described above.

Metal Ion Cell Conditioning—0.1 M solutions (100x) of the indicated metal ions as sulfate, chloride, or bromide salts were prepared in milli-Q purified water. These solutions were prepared directly prior to dosing. Stocks were diluted into cell culture media and cells were treated with dose responses of each metal salt from 1 mM to 1 μM in duplicates for 2 h in 96-well plates then washed with PBS and incubated with 1 μM **3** in cell culture media for 4 h and washed, fixed, and stained as in the puromycin incorporation studies described above.

Redox Cell Conditioning—Reagents previously shown to alter intracellular redox conditions were prepared and dosed in a manner consistent with previous applications[38–43]. FAS was prepared as a 100 mM (100x) stock in deionized water, GSH was prepared as a 0.33 M (300x) stock in water, NAC was prepared as a 10 mM solution in cell culture media, BSO was prepared as a 10 mM (10x) stock in cell culture media, BME was diluted to a 100 mM (1000x) stock in deionized water, Ascorbic acid was prepared as a 1 M (1000x) stock in deionized water, and NADPH was prepared as a 100 mM (100x) stock in deionized water. All stocks were prepared directly prior to dosing and were diluted into cell culture media for dose responses of each reagent in triplicate. Cell were exposed to media containing reagents for the specified amounts of time then washed with PBS and incubated with 1 μM **3** in cell culture media for 4 h and washed, fixed, and stained as in the puromycin incorporation studies described above. To observe changes to GSH levels in cells treated with GSH, NAC, or BSO Abcam fluorometric GSH detection kit (ab138881) was applied according to manufacturer instructions on cell lysates from 96-well plates (ca. 10,000 cells/well) which were treated identically to those assayed with **3**.

Transient Transfection—A standard lipofectamine 2000 (Life Technologies) transient transfection protocol was used for both siRNA and ectopic plasmid DNA transfections.

Briefly, cells were plated the day before transfection. A quarter of the suggested amount of lipofecatamine2000 was used for plasmid transfection. The standard ratio of siRNA:lipofectamine was used for siRNA knockdown experiments. The nucleotide-lipid complexes were added to cells growing in Optimem and allowed to incubate for 6 hours at 37C prior to exchanging into fresh standard growth media for each cell line. Cells were allowed to recover overnight, prior to re-plating for experimental treatments.

PAMPA Assay—Compounds were prepared as 200 μM solutions in 4%DMSO and 10% MeOH in PBS and tested for intrinsic permeability of **2** and **3** across lipid membranes with Corning® Gentest™ Pre-coated PAMPA Plate System (#353015) according to manufacturer instructions. Compound concentrations in donor and acceptor plates were measure via LCMS in single ion mode and calculated from standard curves of each compound prepared in 4%DMSO and 10% MeOH in PBS.

Supplementary Material

Refer to Web version on PubMed Central for supplementary material.

Acknowledgments

References

1. Torti SV, Torti FM. Iron and cancer: more ore to be mined. Nat Rev Cancer. 2013; 13:342–355. [PubMed: 23594855]

2. Bandyopadhyay SK, Chandramouli K, Johnson MK. Iron-sulphur cluster biosynthesis. Biochem Soc Trans. 2008; 36:1112–1119. [PubMed: 19021507]

3. Johnson DC, Dean DR, Smith AD, Johnson MK. Structure, function, and formation of biological iron-sulfur clusters. Annu Rev Biochem. 2005; 74:247–281. [PubMed: 15952888]

4. Kurz T, Eaton JW, Brunk UT. The role of lysosomes in iron metabolism and recycling. Int J Biochem Cell Biol. 2011; 43:1686–1697. [PubMed: 21907822]

5. O'Neill PM, Posner GH. A medicinal chemistry perspective on artemisinin and related endoperoxides. J Med Chem. 2004; 47:2945–2964. [PubMed: 15163175]

6. Mercer AE, et al. Evidence for the involvement of carbon-centered radicals in the induction of apoptotic cell death by artemisinin compounds. J Biol Chem. 2007; 282:9372–82. [PubMed: 17227762]

7. Dixon SJ, Stockwell BR. The role of iron and reactive oxygen species in cell death. Nat Chem Biol. 2014; 10:9–17. [PubMed: 24346035]

8. Pantopoulos K. Iron metabolism and the IRE/IRP regulatory system: an update. Ann NY Acad Sci. 2004; 1012:1–13. [PubMed: 15105251]

9. Wang J, Pantopoulos K. Regulation of cellular iron metabolism. Biochem J. 2011; 434:365–381. [PubMed: 21348856]

10. Richardson DR, Ponka P. The molecular mechanisms of the metabolism and transport of iron in normal and neoplastic cells. Biochim Biophys Acta. 1997; 1331:1–40. [PubMed: 9325434]

11. Fernaeus S, Land T. Increased iron-induced oxidative stress and toxicity in scrapie-infected neuroblastoma cells. Neurosci Lett. 2005; 382:217–220. [PubMed: 15925093]

12. Wessling-Resnick M. Iron Homeostasis and the Inflammatory Response. Annu Rev Nutr. 2010; 30:105–122. [PubMed: 20420524]

13. Boult J, et al. Overexpression of cellular iron import proteins is associated with malignant progression of esophageal adenocarcinoma. Clin Cancer Res. 2008; 14:379–387. [PubMed: 18223212]

14. Kakhlon O, Gruenbaum Y, Cabantchik ZI. Ferritin expression modulates cell cycle dynamics and cell responsiveness to H-ras-induced growth via expansion of the labile iron pool. Biochem J. 2002; 363:431–436. [PubMed: 11964143]

15. Pinnix ZK, et al. Ferroportin and iron regulation in breast cancer progression and prognosis. Sci Transl Med. 2010; 2:43ra56.

16. Wu KJ, Polack A, Dalla-Favera R. Coordinated regulation of iron-controlling genes, H-Ferritin and IRP2, by c-MYC. Science. 1999; 283:676–679. [PubMed: 9924025]

17. Toyokuni S. Role of iron in carcinogenesis: cancer as a ferrotoxic disease. Cancer Sci. 2009; 100:9–16. [PubMed: 19018762]

18. Miller LD, et al. An iron regulatory gene signature predicts outcome in breast cancer. Cancer Res. 2011; 71:6728–6737. [PubMed: 21875943]

19. Kakhlon O, Cabantchik ZI. The labile iron pool: Characterization, measurement, and participation in cellular processes. Free Radic Biol Med. 2002; 33:1037–1046. [PubMed: 12374615]

20. Epsztejn S, et al. Fluorescence analysis of the labile iron pool of mammalian cells. Anal Biochem. 1997; 40:31–40. [PubMed: 9177722]

21. Petrat F, de Groot H, Sustmann R, Rauen U. The chelatable iron pool in living cells: a methodically defined quantity. Biol Chem. 2002; 383:489–502. [PubMed: 12033438]

22. Hirayama T, Okuda K, Nagasawa H. A highly selective turn-on fluorescent probe for iron(II) to visualize labile iron in living cells. Chem Sci. 2013; 4:1250–1256.

23. Au-yeung HY, Chan J, Chantarojsiri T, Chang CJ. Molecular imaging of labile iron(II) pools in living cells with a turn-on fluorescent probe. J Am Chem Soc. 2013; 135:15165–15173. [PubMed: 24063668]

24. Aron AT, Ramos-Torres KM, Cotruvo JA, Chang CJ. Recognition- and reactivity-based fluorescent probes for studying transition metal signaling in living systems. Acc Chem Res. 2015; 48:2434–2442. [PubMed: 26215055]

25. Valecha N, et al. Arterolane, a new synthetic trioxolane for treatment of uncomplicated Plasmodium falciparum malaria: a phase II, multicenter, randomized, dose-finding clinical trial. Clin Infect Dis. 2010; 51:684–91. [PubMed: 20687837]

26. Borstnik K, Paik I, Shapiro TA, Posner GH. Antimalarial chemotherapeutic peroxides: artemisinin, yingzhaosu A and related compounds. Int J Parasitol. 2002; 32:1661–7. [PubMed: 12435451]

27. Valecha N, et al. Arterolane maleate plus piperaquine phosphate for treatment of uncomplicated plasmodium falciparum malaria: a comparative, multicenter, randomized clinical trial. Clin Infect Dis. 2012; 55:663–671. [PubMed: 22586253]

28. Charman SA, et al. Synthetic ozonide drug candidate OZ439 offers new hope for a single-dose cure of uncomplicated malaria. Proc Natl Acad Sci U S A. 2011; 108:4400–4405. [PubMed: 21300861]

29. Creek DJ, et al. Relationship between antimalarial activity and heme alkylation for spiro- and dispiro-1,2,4-trioxolane antimalarials. Antimicrob Agents Chemother. 2008; 52:1291–1296. [PubMed: 18268087]

30. Creek D, et al. Iron-mediated degradation kinetics of substituted dispiro-1, 2, 4- trioxolane antimalarials. J Pharm Sci. 2007; 96:2945–2956. [PubMed: 17549767]

31. Tang Y, et al. Dispiro-1,2,4-trioxane analogues of a prototype dispiro-1,2,4-trioxolane: mechanistic comparators for artemisinin in the context of reaction pathways with iron(II). J Org Chem. 2005; 70:5103–5110. [PubMed: 15960511]

32. Wang X, et al. Spiroadamantyl 1,2,4-trioxolane, 1,2,4-trioxane, and 1,2,4-trioxepane pairs: relationship between peroxide bond iron(II) reactivity, heme alkylation efficiency, and antimalarial activity. Bioorg Med Chem Lett. 2009; 19:4542–4545. [PubMed: 19616946]

33. Mahajan S, et al. A fragmenting hybrid approach for targeted delivery of multiple therapeutic agents to the malaria parasite. Chem Med Chem. 2011; 6:415–419. [PubMed: 21360816]

34. Fontaine SD, Dipasquale AG, Renslo AR. Efficient and stereocontrolled synthesis of 1,2,4-trioxolanes useful for ferrous iron-dependent drug delivery. Org Lett. 2014; 16:5776–5779. [PubMed: 25331549]

35. Fontaine SD, et al. Drug delivery to the malaria parasite using an arterolane-like scaffold. ChemMedChem. 2015; 10:47–51. [PubMed: 25314098]

36. Petrat F, Rauen U, de Groot H. Determination of the chelatable iron pool of isolated rat hepatocytes by digital fluorescence microscopy using the fluorescent probe, phen green SK. Hepatology. 1999; 29:1171–9. [PubMed: 10094962]

37. Chen C, Paw BH. Cellular and mitochondrial iron homeostasis in vertebrates. Biochim Biophys Acta. 2012; 1823:1459–1467. [PubMed: 22285816]

38. Yan CY, Ferrari G, Greene LA. N-acetylcysteine-promoted survival of PC12 cells is glutathione-independent but transcription-dependent. J Biol Chem. 1995; 270:26827–26832. [PubMed: 7592924]

39. Mukherjee TK, Mishra AK, Mukhopadhyay S, Hoidal JR. High concentration of antioxidants N-acetylcysteine and mitoquinone-Q induces intercellular adhesion molecule 1 and oxidative stress by increasing intracellular glutathione. J Immunol. 2007; 178:1835–1844. [PubMed: 17237434]

40. Frikke-Schmidt H, Lykkesfeldt J. Keeping the intracellular vitamin C at a physiologically relevant level in endothelial cell culture. Anal Biochem. 2010; 397:135–137. [PubMed: 19782654]

41. Gao JP, Friedman S, Lanks KW. The role of reduced nicotinamide adenine dinucleotide phosphate in glucose dependent and temperature dependent doxorubicin cytotoxicity. Cancer Chemother Pharmacol. 1993; 33:191–196. [PubMed: 8269599]

42. Ishii T, Sugita Y, Bannai S. Regulation of glutathione levels in mouse spleen lymphocytes by transport of cysteine. J Cell Physiol. 1987; 133:330–336. [PubMed: 3680392]

43. Kang YJ, Feng YI, Hatcher EL. Glutathione Stimulates A549 Cell Proliferation in Glutamine-Deficient Culture : The Effect of Glutamate Supplementation. J Cell Physiol. 1994; 161:589–596. [PubMed: 7962140]

44. Espósito BP, Epsztejn S, Breuer W, Cabantchik ZI. A review of fluorescence methods for assessing labile iron in cells and biological fluids. Anal Biochem. 2002; 304:1–18. [PubMed: 11969183]

45. Martins MM, et al. Linking tumor mutations to drug responses via a quantitative chemical-genetic interaction map. Cancer Discov. 2015; 5:154–167. [PubMed: 25501949]
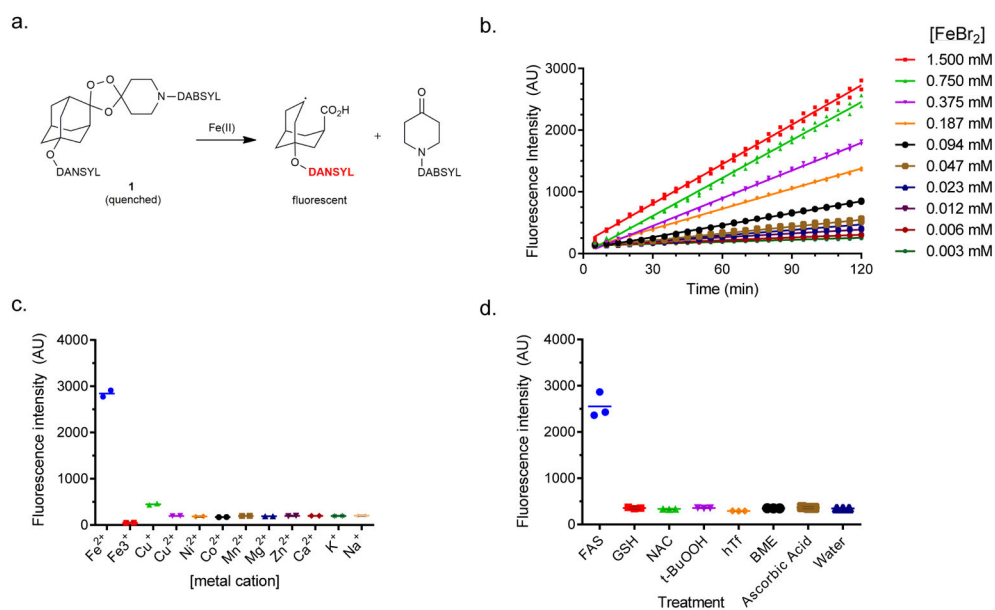
Figure 1. A turn-on fluorescent probe reveals Fe(II)-selective reactivity of trioxolanes
(**a**) Chemical structure and mechanism of turn-on fluorescent probe **1**. (**b**) Fluorescence signal at 465 nm (E_{max}) of trioxolane-based fluorescent probe **1** over time when exposed to the indicated concentrations of $FeBr_2$. (n=2, error bars represent s.e.m.). (**c**) Fluorescence signal at 465 nm of **1** when treated with 1.5 mM (1 M for Na^+) solutions of the indicated metal ions for 2 hours. (n=2). (**d**) Fluorescence signal at 465 nm of **1** when treated with 3 mM solutions of the indicated biologically relevant redox-active reagents for 5 hours. (n=3).
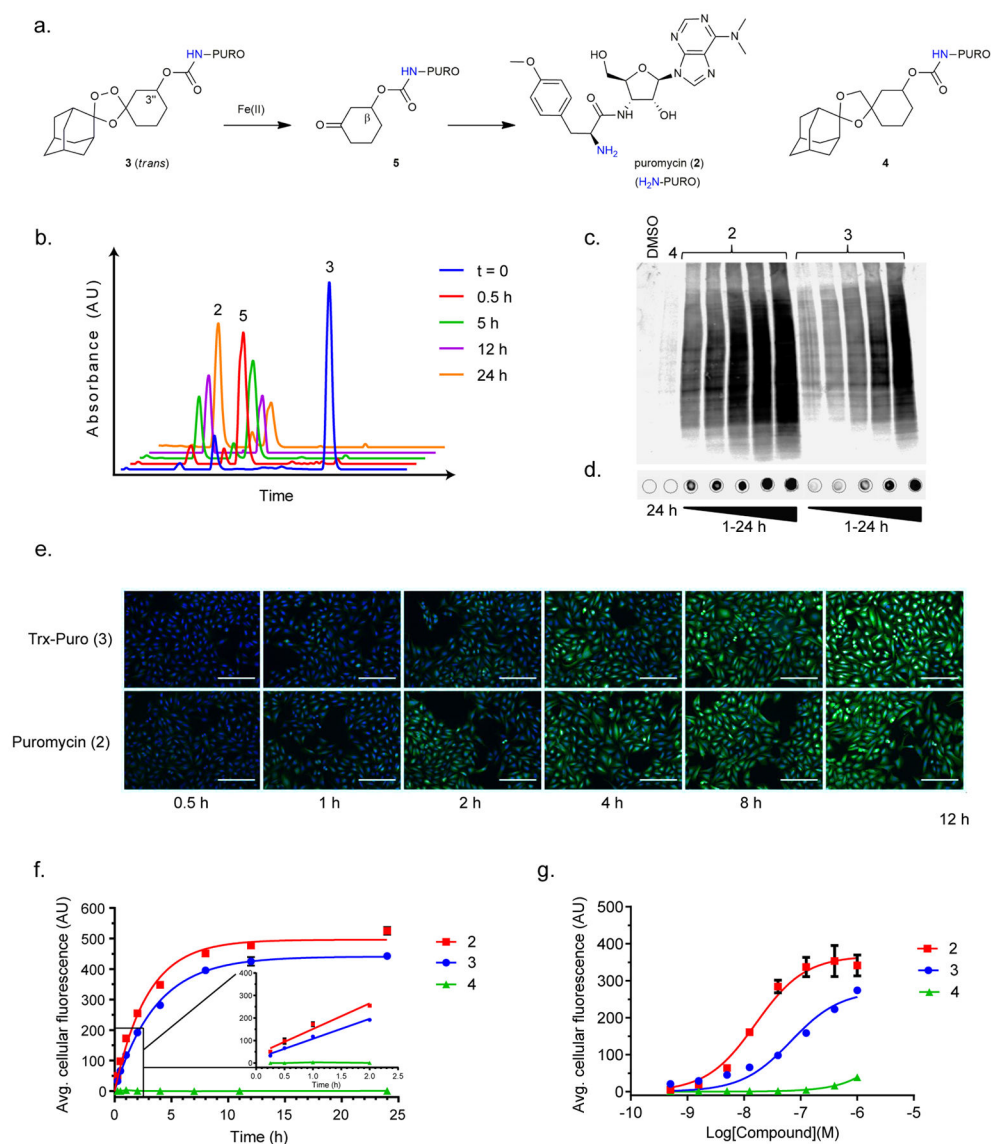
Figure 2. Trioxolane-conjugate of puromycin as a cellular probe of Fe(II)

(**a**) Chemical structure of probe **3** and mechanism of puromycin (**2**) release as well as the structure of dioxolane control **4**. (**b**) LCMS spectra (UV absorbance at 275 nm) illustrating the reaction of **3** with FAS in cell-culture media to yield **5** and then **2**. (**c**) Incorporation of puromycin in cellular proteins of U-2 OS cells treated with 1 μM solutions of **2**, **3**, or **4** as assessed by Western or (**d**) dot blot analysis with anti-puromycin antibodies. (**e**) Immunofluorescence images showing puromycin incorporation in U-2 OS cells treated with 0.1 μM solutions of **3** or free puromycin (**2**). Scale bars denote 200 μm. (**f**) High-content image quantification of average cellular puromycin incorporation from over 2000 cells per condition in U-2 OS cells treated with 0.1 μM solutions of **2**, **3**, or **4**. The mean cellular intensity under each condition is reported across experimental triplicates with error bars depicting +/− s.e.m. The inset shows initial rates of puromycin incorporation in the linear regime (7.4 and 3.7 AU/h for **2** and **3** respectively). The initial incorporation rate in cells

treated with control **4** was indistinguishable from zero. (**g**) Quantification of average cellular puromycin incorporation in cells treated in dose response with **2**, **3**, or **4** for 8 h then fixed, stained, and imaged as in (e) and (f). Values represent the well mean intensity values across experimental triplicates as in (f) with error bars depicting +/− s.e.m.
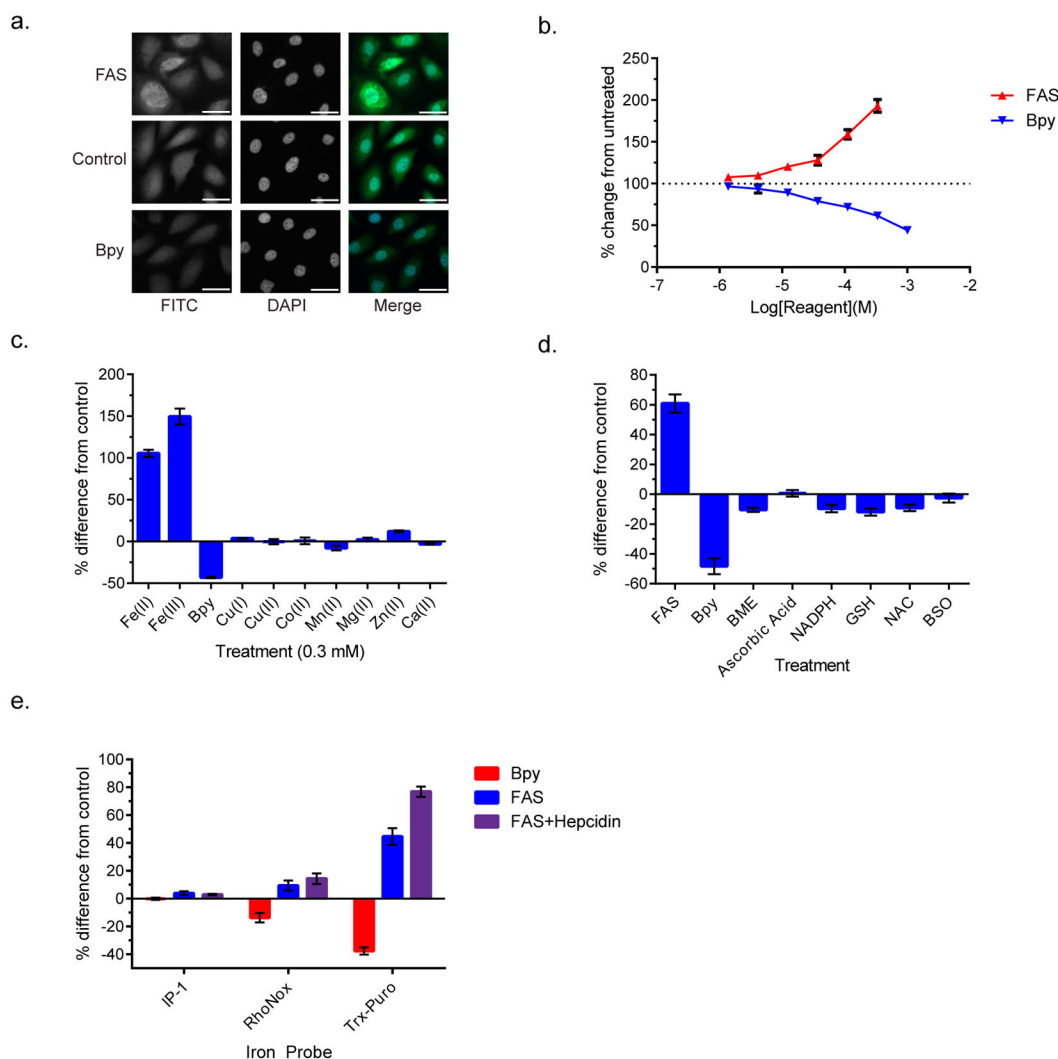
Figure 3. Reactivity-based probe 3 is highly selective for Fe(II) in cells
(**a**) Representative images of PC-3 cells pre-treated with FAS (0.3 mM), Bpy (1 mM), or vehicle for 2 h then washed and exposed to 1 μM of **3** for 4 h. Puromycin incorporation is visualized in the FITC channel (green), nuclei in the DAPI channel (blue). Scale bars denote 50 μm. (**b**) Average cellular puromycin incorporation in PC-3 cells pretreated with FAS or Bpy for 2 h then washed with PBS and exposed to 1 μM **3** for 4 h. Greater than 2000 cells were imaged and analyzed per condition and mean cellular intensity is reported across experimental triplicates with error bars depicting +/− s.e.m. (**c**) Average cellular puromycin incorporation in PC-3 cells pretreated with 0.3 mM solutions of the indicated metal ions for 2 h then washed and probed with **3** as described in (b). (**d**) Average cellular puromycin incorporation in PC-3 cells treated pretreated with solutions of GSH (1 mM for 22 h), NAC (10 mM for 20 h), BSO (1 mM for 20 h), BME (0.1 mM for 20 h), ascorbic Acid (1 mM for 3 h), or NADPH (1 mM for 3 h) in cell culture media and then washed and probed with **3** as described in (b). (**e**) Relative response of three iron probes when applied to PC-3 cells treated with 0.3 mM FAS, Bpy, or FAS after pretreatment with Hepcidin. Cells imaged and analyzed as described in (b).
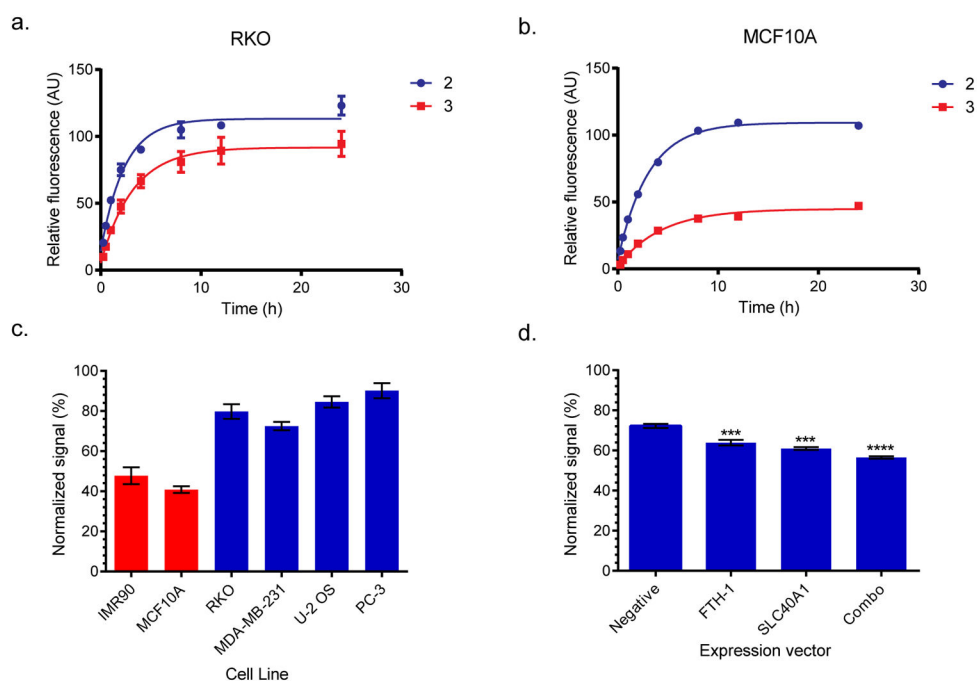
Figure 4. Comparing reactive Fe(II) pools across cell lines and genetic modulations
(**a**) Puromycin incorporation over time in RKO cells treated with 0.1 μM solutions of **2** or **3** in cell culture medium. Background in vehicle treated cells is subtracted and data is normalized to puromycin incorporation at saturation in cells treated with free puromycin. More than 10,000 cells were imaged and analyzed per condition; mean cellular intensity under each condition is reported across experimental triplicates with error bars depicting +/– s.e.m. (**b**) Puromycin incorporation over time in MCF10A cells treated with 0.1 μM solutions of **2** or **3**. Greater than 2500 cells were imaged and analyzed as described in (a). (**c**) Puromycin incorporation at saturation in cells treated with 0.1 μM **3** normalized to that in cells treated with equimolar free puromycin (**2**) across cell lines from diverse origins. Non-tumorigenic cell lines are indicated in red with cancer derived cell lines shown in blue. Data generated from experimental triplicates with error bars depicting +/– s.e.m. (**d**) Reactive iron pools in RKO cells transiently transfected with expression vectors for ferritin, ferroportin, or the combination of the two. Normalized signal represents average cellular puromycin incorporation at saturation in **3**-treated cells (0.1 μM) normalized to signal in **2**-treated cells (0.1 μM). Greater than 5000 cells were analyzed per condition as describe in (b). Asterisk represent statistical significance of difference from negative control (one-way ANOVA with Dunnett's test): *** = p < 0.001, **** = p < 0.0001.